Syntheses, Structures, and Berry Pseudorotation of Ruthenium−Phosphorane Complexes

Hiroshi Nakazawa,* Kazumori Kawamura, Kazuyuki Kubo, and Katsuhiko Miyoshi*

Department of Chemistry, Faculty of Science, Hiroshima University, Higashi-Hiroshima 739-8526, Japan

Received January 25, 1999

Ruthenium complexes containing a hypervalent phosphorus ligand, $[Cp(CO)_2Ru\{P(OC_6H_4E)_2\}]$ (E = NH (**2a**), NMe (**2b**), or O (**4a**)), $[Cp(CO)_2Ru\{P(OC_{10}H_6O)_2\}]$ (**4b**), and $[Cp(CO)_2Ru\{P(OC_7H_6O)_2\}]$ (**4c**), were prepared in the reaction of $[Cp(CO)_2Ru\{P(OPh)_3\}]BF_4$ (**1**) with the corresponding aryl alcohol or arylamine and Et_3N or *n*-BuLi. The comparison of spectroscopic data of $[Cp(CO)_2M\{P(OC_6H_4E)_2\}]$ (M = Ru, Fe) (E = NH, NMe, O) reveals that the Ru−P bonding is more polarized as $M^{\delta+}-P^{\delta-}$ than the Fe−P bonding. During the course of preparation of **2b**, a phosphite complex $[Cp(CO)_2Ru\{P(OC_6H_4NMe)(OC_6H_4NMeH)\}]BF_4$ (**3**) was isolated, which reacted with a Lewis base to give **2b**. The X-ray structures of **2b**, **4b**, and **3** were determined. **2b** and **4b** have slightly distorted trigonal-bipyramidal geometries. From the variable-temperature ^{31}P NMR study for **4c**, the activation parameters for Berry pseudorotation around the pentacoordinate phosphorus were determined to be $\Delta H^{\ddagger} = 42.1 \pm 0.5$ kJ mol^{-1}, $\Delta S^{\ddagger} = -91.1 \pm 1.6$ J mol^{-1} K^{-1}, and $\Delta G_{340}{}^{\ddagger} = 73.1 \pm 0.7$ kJ mol^{-1}. This constitutes the first determined activation parameters of Berry pseudorotation for a metallaphosphorane complex.

Introduction

Metalated derivatives of pentacoordinate phosphorus compounds, metallaphosphoranes, have received considerable attention because they have a hypervalent 3-center 4-electron bond. Several kinds of methods for the preparation of metallaphosphoranes have been reported: (1) deprotonation[1] and (2) protonation[2] at a nitrogen in polycyclic species with phosphine− and/or amine−metal bonds, (3) oxidative addition of halogen to transition-metal phosphide complexes[3] (and Sb and As versions[4]), (4) nucleophilic substitution at a phosphorane phosphorus atom by a transition-metal anion,[5] and (5) electrophilic attack of an electron-deficient transition-metal fragment at a phosphoranide[6] (and the Sb version[7]). Some other preparative methods[8] and review articles[9] have been reported. We recently reported an unprecedented method for the preparation of iron−phosphorane complexes (Scheme 1), involving the nucleophilic attack of an organic nucleophile at a trivalent phosphorus coordinated to an iron.[10] To expand the scope of this preparative method, we examined reactions of a ruthenium complex, $[Cp(CO)_2Ru\{P(OPh)_3\}]^+$. This paper reports preparations, properties, X-ray structures, and pseudorotation of ruthenium phosphoranes, $Cp(CO)_2Ru\{P(OC_6H_4E)_2\}$ ($Cp = \eta^5$-C_5H_5; E = NH, NMe, O; although the complex should be described as $Cp(CO)_2Ru\{P(OC_6H_4E)_2\}$, the tie bar is omitted hereafter for simplicity), and some related complexes.

(1) (a) Wachter, J.; Mentzen, B. F.; Riess, J. G. *Angew. Chem., Int. Ed. Engl.* **1981**, *20*, 284. (b) Vierling, P.; Riess, J. G. *J. Am. Chem. Soc.* **1981**, *103*, 2466. (c) Jeanneaux, F.; Grand, A.; Riess, J. G. *J. Am. Chem. Soc.* **1981**, *103*, 4272. (d) Dupart, J.-M.; Grand, A.; Pace, S.; Riess, J. G. *J. Am. Chem. Soc.* **1982**, *104*, 2316. (e) Vierling, P.; Riess, J. G. *J. Am. Chem. Soc.* **1984**, *106*, 2432. (f) Dupart, J.-M.; Grand, A.; Riess, J. G. *J. Am. Chem. Soc.* **1986**, *108*, 1167. (g) Vierling, P.; Riess, J. G. *Organometallics* **1986**, *5*, 2543. (h) Vierling, P.; Riess, J. G.; Grand, A. *Inorg. Chem.* **1986**, *25*, 4144. (i) Khasnis, D. V.; Burton, J. M.; Zhang, H.; Lattman, M. *Organometallics* **1992**, *11*, 3745.

(2) (a) Khasnis, D. V.; Lattman, M.; Siriwardane, U. *Inorg. Chem.* **1989**, *28*, 681. (b) Khasnis, D. V.; Lattman, M.; Siriwardane, U. *Inorg. Chem.* **1989**, *28*, 2594. (c) Khasnis, D. V.; Lattman, M.; Siriwardane, U. *J. Chem. Soc., Chem. Commun.* **1989**, 1538. (d) Khasnis, D. V.; Lattman, M.; Siriwardane, U.; Chopra, S. K. *J. Am. Chem. Soc.* **1989**, *111*, 3103. (e) Khasnis, D. V.; Lattman, M.; Siriwardane, U. *Organometallics* **1991**, *10*, 1326. (f) Khasnis, D. V.; Lattman, M.; Siriwardane, U.; Zhang, H. *Organometallics* **1992**, *11*, 2074.

(3) (a) Ebsworth, E. A. V.; McManus, N. T.; Pilkington, N. J.; Rankin, D. W. H. *J. Chem. Soc., Chem. Commun.* **1983**, 484. (b) Ebsworth, E. A. V.; Holloway, J. H.; Pilkington, N. J.; Rankin, D. W. H. *Angew. Chem., Int. Ed. Engl.* **1984**, *23*, 630.

(4) Malisch, W.; Kaul, H. A.; Gross, E.; Thewalt, U. *Angew. Chem., Int. Ed. Engl.* **1982**, *21*, 549.

(5) (a) Lattman, M.; Anand, B. N.; Garrett, D. R.; Whitener, M. A. *Inorg. Chim. Acta* **1983**, *76*, L139. (b) Lattman, M.; Morse, S. A.; Cowley, A. H.; Lasch, J. G.; Norman, N. C. *Inorg. Chem.* **1985**, *24*, 1364. (c) Anand, B. N.; Bains, R.; Usha, K. *J. Chem. Soc., Dalton Trans.* **1990**, 2315.

(6) Chopra, S. K.; Martin, J. C. *Heteroatom Chem.* **1991**, *2*, 71.

(7) Yamamoto, Y.; Okazaki, M.; Wakisaka, Y.; Akiba, K.-y. *Organometallics* **1995**, *14*, 3364.

(8) (a) Lattman, M.; Chopra, S. K.; Cowley, A. H.; Arif, A. M. *Organometallics* **1986**, *5*, 677. (b) Burns, E. G.; Chu, S. S. C.; Meester, P.; Lattman, M. *Organometallics* **1986**, *5*, 2383. (c) Lattman, M.; Burns, E. G.; Chopra, S. K.; Cowley, A. H.; Arif, A. M. *Inorg. Chem.* **1987**, *26*, 1926.

(9) (a) Montgomery, C. D. *Phosphorus, Sulfur, Silicon* **1993**, *84*, 23. (b) Dillon, K. B. *Chem. Rev.* **1994**, *94*, 1441.

(10) (a) Nakazawa, H.; Kubo, K.; Miyoshi, K. *J. Am. Chem. Soc.* **1993**, *115*, 5863. (b) Kubo, K.; Nakazawa, H.; Mizuta, T.; Miyoshi, K. *Organometallics* **1998**, *17*, 3522.

10.1021/om990044k CCC: $18.00
Publication on Web 07/03/1999

Scheme 1

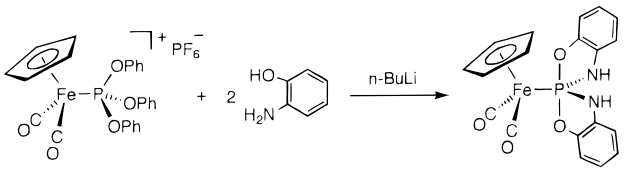

Experimental Section

General Remarks. All reactions were carried out under an atmosphere of dry nitrogen by using standard Schlenk tube techniques. All solvents were purified by distillation: Ether, THF, benzene, toluene, and *p*-xylene were distilled from sodium/benzophenone, hexane and pentane were distilled from sodium metal, and CH_2Cl_2 was distilled from P_2O_5. Acetone was dried with anhydrous $CaSO_4$ and distilled. They were stored under an N_2 atmosphere. Other reagents were used as received. $Cp(CO)_2RuCl$,[11] $HP(OC_6H_4NH)_2$,[12] and *o*-$C_6H_4(NHMe)(OH)$[13] were prepared according to the respective published procedures.

IR spectra were recorded on Shimadzu FTIR-4000 and FTIR-8100A spectrometers. ^1H, ^{13}C, and ^{31}P NMR spectra were measured on JEOL EX-270, EX-400, and LA-300 spectrometers. ^1H NMR and ^{13}C NMR data were referenced to $Si(CH_3)_4$ as an internal standard. ^{31}P NMR data were referenced to 85% H_3PO_4 as an external standard. Elemental analyses were performed on a Perkin-Elmer 2400CHN elemental analyzer.

Preparation of $[Cp(CO)_2Ru\{P(OPh)_3\}]BF_4$ (1). A solution of $Cp(CO)_2RuCl$ (2860 mg, 11.10 mmol) and $P(OPh)_3$ (3445 mg, 11.10 mmol) in CH_2Cl_2 (100 mL) was added to a suspension of $AgBF_4$ (2162 mg, 11.10 mmol) in CH_2Cl_2 (20 mL). The mixture was stirred for 24 h at room temperature. After filtration to remove AgCl formed, the solvent was removed from the filtrate under reduced pressure to give a yellow powder, which was washed with benzene and then ether. Recrystallization from CH_2Cl_2/hexane gave colorless crystals of **1** (6145 mg, 9.92 mmol, 89%). Anal. Calcd for $C_{25}H_{20}BF_4O_5PRu$: C, 48.49; H, 3.26. Found: C, 48.29; H, 3.35.

Preparation of $[Cp(CO)_2Ru\{P(OC_6H_4NH)_2\}]$ (2a) from 1. A solution of **1** (619 mg, 1.00 mmol) in THF (10 mL) was added to a solution of *o*-$C_6H_4(NH_2)(OH)$ (218 mg, 2.00 mmol) and Et_3N (0.14 mL, 1.00 mmol) in THF (5 mL). The mixture was stirred for 4 h at 60 °C, and the volatiles were removed under reduced pressure. The yellow residue was extracted with hot ether (50 mL × 4), and the ether extract was evaporated to dryness. The resulting solid was washed with ether (2 mL × 5) and dried in vacuo to yield a white powder of **2a** (238 mg, 0.51 mmol, 51%). Anal. Calcd for $C_{19}H_{15}N_2O_4PRu$: C, 48.83; H, 3.23; N, 5.99. Found: C, 48.59; H, 3.36; N, 5.81.

Preparation of $[Cp(CO)_2Ru\{P(OC_6H_4NH)_2\}]$ (2a) from $Cp(CO)_2RuCl$ and $HP(OC_6H_4NH)_2$. A solution of $HP(OC_6H_4NH)_2$ (626 mg, 2.54 mmol) in THF (5 mL) was treated with *n*-BuLi (2.37 mL of *n*-BuLi, 1.61 M hexane solution, 3.81 mmol) at −78 °C. The colorless solution changed immediately to a white suspension. After it had been stirred at −78 °C for 20 min, the reaction mixture was treated with $Cp(CO)_2RuCl$ (657 mg, 2.55 mmol) and was warmed to room temperature and then stirred for 24 h to complete the reaction. The solvent was removed under reduced pressure, and the residue was extracted with hot ether (50 mL × 4). After the ether extract was dried in vacuo, the resulting white powder was washed with a small amount of ether and dried in vacuo to give **2a** (224 mg, 0.48 mmol, 19%).

Preparation of $[Cp(CO)_2Ru\{P(OC_6H_4NMe)_2\}]$ (2b) from 1. A solution of *o*-$C_6H_4(NHMe)(OH)$ (200 mg, 1.62 mmol) in THF (5 mL) was treated with *n*-BuLi (0.50 mL of *n*-BuLi, 1.61 M of hexane solution, 0.81 mmol) at −78 °C. After it had been stirred at −78 °C for 20 min, the reaction mixture was treated with **1** (502 mg, 0.81 mmol) and warmed to room temperature and then stirred for 4 h. The solvent was removed under reduced pressure, and the residue was washed with a small amount of ether and then extracted with hot ether (20 mL × 4). The ether extract was concentrated to ca. 3 mL and cooled to −10 °C, yielding yellow crystals of **2b** (99 mg, 0.20 mmol, 25%). Anal. Calcd for $C_{21}H_{19}N_2O_4PRu$: C, 50.91; H, 3.87; N, 5.65. Found: C, 51.03; H, 3.95; N, 5.72.

Preparation of $[Cp(CO)_2Ru\{P(OC_6H_4NMe)_2\}]$ (2b) from 3. A white suspension of **3** (100 mg, 0.17 mmol) in THF (2 mL) was treated with Et_3N (0.024 mL, 0.17 mmol) at room temperature. The mixture was stirred for 8 h to give a yellow solution. The solvent was removed under reduced pressure. The resulting solid was extracted with hot ether (15 mL × 5), and the ether extract was concentrated to ca. 3 mL. Cooling to −10 °C yielded yellow crystals of **2b** (65 mg, 0.13 mmol, 77%).

Preparation of $[Cp(CO)_2Ru\{P(OC_6H_4NMe)(OC_6H_4NHMe)\}]BF_4$ (3). A solution of *o*-$C_6H_4(NHMe)(OH)$ (505 mg, 4.10 mmol) in THF (5 mL) was treated with *n*-BuLi (1.27 mL of *n*-BuLi, 1.61 M of hexane solution, 2.05 mmol) at −78 °C. After it had been stirred at −78 °C for 20 min, the reaction mixture was treated with **1** (1197 mg, 1.93 mmol), warmed to room temperature, and then stirred for ca. 24 h until the yellow solution was changed to a white suspension. A precipitate was collected by filtration, washed with cold THF, and dissolved in acetone (20 mL). After filtration to remove insoluble materials, the solvent was removed in vacuo to give a white powder of **3** (891 mg, 1.53 mmol, 79%). Anal. Calcd for $C_{21}H_{20}BF_4N_2O_4PRu$: C, 43.25; H, 3.46; N, 4.80. Found: C, 42.99; H, 3.44; N, 4.79.

Preparation of $[Cp(CO)_2Ru\{P(OC_6H_4O)_2\}]$ (4a). A solution of **1** (520 mg, 0.84 mmol) in THF (5 mL) was added to a solution of *o*-$C_6H_4(OH)_2$ (185 mg, 1.68 mmol) and Et_3N (0.12 mL, 0.84 mmol) in THF (3 mL). The mixture was stirred for 4 h at 60 °C, and the volatiles were removed under reduced pressure. The yellow residue was extracted with hot ether (20 mL × 4), and the ether extract was evaporated to dryness. The resulting solid was washed with ether (1 mL × 5) and dried in vacuo to yield a white powder of **4a** (304 mg, 0.65 mmol, 77%). Anal. Calcd for $C_{19}H_{13}O_6PRu$: C, 48.62; H, 2.79. Found: C, 48.54; H, 2.96.

Preparation of $[Cp(CO)_2Ru\{P(OC_{10}H_6O)_2\}]$ (4b). A treatment of **1** (329 mg, 0.53 mmol) with 2,3-$C_{10}H_6(OH)_2$ (170 mg, 1.06 mmol) and Et_3N (0.074 mL, 0.53 mmol) in a manner similar to that of **4a** gave a white powder of **4b** (196 mg, 0.34 mmol, 65%). Anal. Calcd for $C_{27}H_{17}O_6PRu$: C, 62.24; H, 4.66; N, 5.18. Found: C, 62.09; H, 4.71; N, 5.04.

Preparation of $[Cp(CO)_2Ru\{P(OC_7H_6O)_2\}]$ (4c). A treatment of **1** (596 mg, 0.96 mmol) with 3-methylcatechol (239 mg, 1.93 mmol) and Et_3N (0.13 mL, 0.96 mmol) in a manner similar to that of **4a** gave a white powder of **4c** (312 mg, 0.63 mmol, 66%). Anal. Calcd for $C_{21}H_{17}O_6PRu$: C, 50.71; H, 3.44. Found: C, 50.66; H, 3.44.

X-ray Structure Determination for 2b, 4b, and 3. Single crystals of **2b** grown from ether, **4b** grown from toluene/hexane, and **3** grown from CH_2Cl_2/hexane in a refrigerator were individually mounted on an Enraf-Nonius CAD4 diffractometer and irradiated with graphite-monochromated Mo Kα radiation ($\lambda = 0.710\ 73$ Å). Unit cell dimensions were obtained by least-squares from the angular setting of 25 carefully centered reflections with $23° < 2\theta < 36°$ for **2b**, from that of 15 such reflections with $20° < 2\theta < 22°$ for **4b**, and from that of 24 such reflections with $21° < 2\theta < 36°$ for **3**. $P2/c$, $P2_12_12_1$, and $P2_1/n$ were selected as the space groups for **2b**, **4b**, and **3**, respectively, which led to successful refinements. Reflection

(11) Blockmore, T.; Cottton, J. D.; Bruce, M. I.; Stone, F. G. A. *J. Chem. Soc. A* **1968**, 2931.
(12) Malavaud, C.; Charbonnel, Y.; Barrans, J. *Tetrahedron Lett.* **1975**, 497.
(13) Anderson, G. W.; Bell, F. *J. Chem. Soc.* **1949**, 2668.

Scheme 2

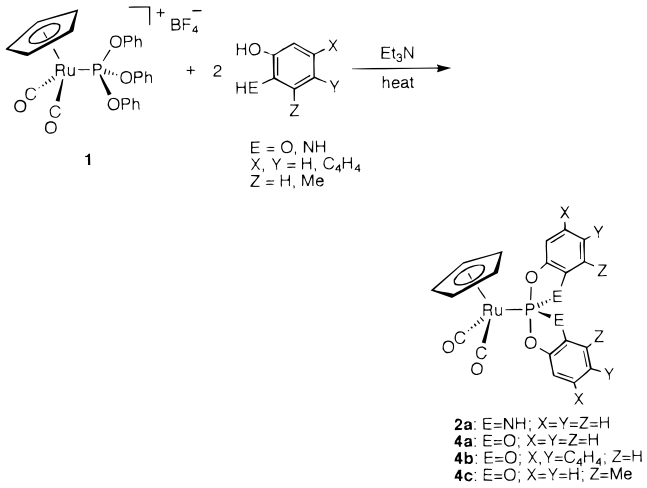

Scheme 3

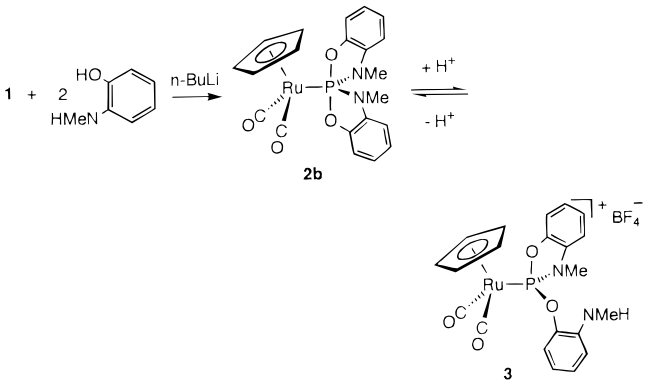

Scheme 4

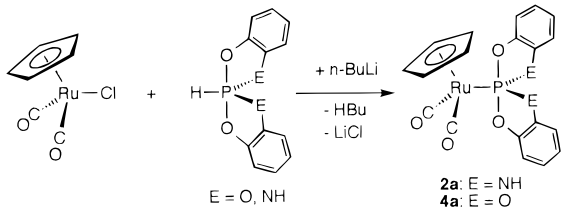

intensities were collected in the usual manner at 20 ± 1 °C, and 3 representative reflections checked after every 200 reflections showed no decrease in intensity.

The structure was solved by a heavy-atom Patterson method with the PATTY program system[14] for **2b** and by direct methods with the SHELXS86 program system[15] for **4b** and **3**. The positions of all hydrogen atoms were calculated by assuming idealized geometries. For **3**, the counteranion, BF_4^-, was refined as a disordered molecule. Absorption and extinction corrections were then applied, and several cycles of a full-matrix least-squares refinement with anisotropic temperature factors for non-hydrogen atoms led to final values of $R = 0.027$ and $R_w = 0.036$ for **2b**, $R = 0.048$ and $R_w = 0.035$ for **4b**, and $R = 0.058$ and $R_w = 0.047$ for **3**. All calculations were performed using teXsan.[16]

Results and Discussion

Preparation and Characterization of Ruthenium−Phosphorane Complexes. Ruthenium complexes containing a phosphorane fragment were synthesized according to the method reported previously for the corresponding iron complexes[10] with some modifications. $[Cp(CO)_2Ru\{P(OPh)_3\}]BF_4$ (**1**) was added to a reaction mixture of 2 equiv of *o*-$C_6H_4(NH_2)(OH)$ and 1 equiv of Et_3N in THF, and then the reaction mixture was heated at 60 °C to give a white powder (Scheme 2). We concluded that the product is a ruthenium−phosphorane, $[Cp(CO)_2Ru\{P(OC_6H_4NH)_2\}]$ (**2a**), from the following spectroscopic data similar to those of the iron analogue:[10] (i) Two IR absorption bands due to ν_{CO} (2037 and 1983 cm^{-1}) were observed in a terminal carbonyl region of electrically neutral complexes. (ii) In the ^{31}P NMR spectrum, one resonance was observed at 0.66 ppm, which is at a higher field by 136 ppm than that of the starting complex, as a singlet with proton irradiation and as a triplet with $J = 18.0$ Hz without proton irradiation, indicating the formation of a pentavalent pentacoordinate phosphorus with two NHR groups directly bonded to it. (iii) In the ^1H NMR spectrum, in addition to a doublet due to Cp protons and multiplet due to phenyl protons, a doublet assigned to NH protons was observed at 5.27 ppm with $J = 17.6$ Hz.

Similarly, $[Cp(CO)_2Ru\{P(OC_6H_4O)_2\}]$ (**4a**), $[Cp(CO)_2Ru\{P(OC_{10}H_6O)_2\}]$ (**4b**), and $[Cp(CO)_2Ru\{P(OC_7H_6O)_2\}]$ (**4c**) were prepared from **1** and *o*-$C_6H_4(OH)_2$, 2,3-$C_{10}H_6(OH)_2$, and 3-methylcatechol, respectively (Scheme 2). In all cases, the reactions proceeded cleanly, but the yields of the isolated complexes were in the range of 51−77%, depending on the solubility and crystallinity of the respective complexes.

The formation mechanism of the ruthenium phosphoranes can be considered to be the same as that of iron phosphoranes.[10] That is, it involves nucleophilic attacks of an organic nucleophile such as ^-OR or $^-NR_2$ at a trivalent phosphorus coordinated to a ruthenium and the subsequent substitutions on the phosphorus.

In the reaction of **1** with *o*-$C_6H_4(NHMe)(OH)$ and *n*-BuLi at room temperature, a quantitative formation of $[Cp(CO)_2Ru\{P(OC_6H_4NMe)_2\}]$ (**2b**) is confirmed first in the ^{31}P NMR spectrum of the reaction mixture, and then **2b** changes to the corresponding phosphite complex, $[Cp(CO)_2Ru\{P(OC_6H_4NMe)(OC_6H_4NHMe)\}]BF_4$ (**3**) (Scheme 3). Preparation of **2b** by this method leads to the concomitant formation of 3 equiv of PhOH, which reacts with the more basic N atom in **2b**, compared with that of **2a**, to give a cationic complex **3**. An equilibrium between **2b** and **3** may exist in solution, but **3** is readily precipitated out from the solution, which makes **3** a main product in this reaction. The reaction of isolated **3** with a base such as Et_3N gives **2b** in a good yield (77%).

Another method for the preparation of metallaphosphoranes, which has been reported for an iron analogue, is a replacement of chloride on a transition metal by phosphoranide.[6,10] This method was applied for the preparation of **2a** and **4a** (Scheme 4). The reaction of $Cp(CO)_2RuX$ (X = Cl, I) with hydridophosphorane $HP(OC_6H_4E)_2$ (E = NH, O) in the presence of a base gave

(14) PATTY: Beurskens, P. T.; Admiraal, G.; Beurskens, G.; Bosman, W. P.; Garcia-Granda, S.; Gould, R. O.; Smits, J. M. M.; Smykalla, C. *The DIRDIF program system*; Technical Report of the Crystallography Laboratory, University of Nijmegen: Nijmegen, The Netherlands, 1992.

(15) SHELXS86: Sheldrick, G. M. In *Crystallographic Computing 3*; Sheldrick, G. M., Kruger, C., Goddard, R., Eds.; Oxford University Press: New York, 1985; pp 175−189.

(16) teXsan: *Crystal Structure Analysis Package*; Molecular Structure Corp.: The Woodlands, TX, 1985, 1992.

Table 1. Spectroscopic Data

complex	IR (THF): ν_{CO} (cm^{-1})	^1H NMR ($CDCl_3$): δ (ppm)	^{13}C NMR ($CDCl_3$): δ (ppm)	^{31}P NMR ($CDCl_3$): δ (ppm)
1	2083	5.21 (s, 5H, C_5H_5)	89.41 (s, C_5H_5)	136.50 (s)
	2037	7.18−7.25 (m, 9H, OC_6H_5)	120.88 (d, J_{PC} = 5.0 Hz, *o*-C_6H_5)	
		7.37−7.42 (m, 6H, OC_6H_5)	126.84 (s, *p*-C_6H_5)	
			130.73 (s, *m*-C_6H_5)	
			149.72 (d, J_{PC} = 8.1 Hz, ϵ-C_6H_5)	
			191.56 (d, J_{PC} = 21.8 Hz, CO)	
2a	2037	5.27 (d, J_{PH} = 17.6 Hz, 2H, NH)	88.59 (s, C_5H_5)[a]	0.66 (s)
	1983	5.38 (s, 5H, C_5H_5)	108.88 (d, J_{PC} = 12.9 Hz, OC_6H_4N)	
		6.59−6.67 (m, 8H, OC_6H_4N)	109.03 (s, OC_6H_4N)	
			119.07 (s, OC_6H_4N)	
			119.64 (s, OC_6H_4N)	
			132.79 (d, J_{PC} = 14.7 Hz, OC_6H_4N)	
			149.21 (d, J_{PC} = 3.7 Hz, OC_6H_4N)	
			197.98 (d, J_{PC} = 22.1 Hz, CO)	
			198.20 (d, J_{PC} = 22.0 Hz, CO)	
2b	2036	3.27 (d, J_{PH} = 8.9 Hz, 6H, NCH_3)	32.81 (d, J_{PC} = 3.7 Hz, NCH_3)	−6.93 (s)
	1983	5.38 (d, J_{PH} = 1.3 Hz, 5H, C_5H_5)	87.40 (d, J_{PC} = 2.5 Hz, C_5H_5)	
		6.61 (d, J_{HH} = 7.9 Hz, 2H, OC_6H_4N)	107.51 (s, OC_6H_4N)	
		6.70−6.87 (m, 6H, OC_6H_4N)	107.58 (d, J_{PC} = 9.8 Hz, OC_6H_4N)	
			118.15 (s, OC_6H_4N)	
			119.01 (s, OC_6H_4N)	
			136.43 (d, J_{PC} = 18.2 Hz, OC_6H_4N)	
			148.45 (d, J_{PC} = 7.3 Hz, OC_6H_4N)	
			197.04 (d, J_{PC} = 20.8 Hz, CO)	
			197.82 (d, J_{PC} = 23.2 Hz, CO)	
3	2084	2.85 (s, 3H, NHCH_3)[b]	29.50 (d, J_{PC} = 11.8 Hz, $PNCH_3$)[b]	147.71 (s)[b]
	2038	3.43 (d, J_{PH} = 12.0 Hz, 3H, $PNCH_3$)	30.73 (s, $NHCH_3$)	
		4.88 (s, 1H, N*H*CH_3)	91.98 (d, J_{PC} = 1.9 Hz, C_5H_5)	
		6.16 (d, J_{PH} = 0.8 Hz, 5H, C_5H_5)	110.17 (d, J_{PC} = 6.8 Hz, OC_6H_4N)	
		6.36−7.20 (m, 8H, OC_6H_4N)	112.66 (d, J_{PC} = 6.2 Hz, OC_6H_4N)	
			112.92 (d, J_{PC} = 1.8 Hz, OC_6H_4N)	
			117.20 (s, OC_6H_4N)	
			121.89 (s, OC_6H_4N)	
			122.20 (d, J_{PC} = 4.4 Hz, OC_6H_4N)	
			125.27 (s, OC_6H_4N)	
			128.59 (d, J_{PC} = 1.9 Hz, OC_6H_4N)	
			136.67 (d, J_{PC} = 6.8 Hz, OC_6H_4N)	
			139.44 (d, J_{PC} = 13.7 Hz, OC_6H_4N)	
			142.58 (d, J_{PC} = 3.7 Hz, OC_6H_4N)	
			148.97 (d, J_{PC} = 9.3 Hz, OC_6H_4N)	
			193.79 (d, J_{PC} = 22.4 Hz, CO)	
			194.03 (d, J_{PC} = 21.8 Hz, CO)	
4a	2052	5.41 (d, J_{PH} = 1.3 Hz, 5H, C_5H_5)	87.89 (d, J_{PC} = 2.5 Hz, C_5H_5)	47.82 (s)
	2001	6.80−6.94 (m, 8H, OC_6H_4O)	110.31 (d, J_{PC} = 9.8 Hz, OC_6H_4O)	
			120.99 (s, OC_6H_4O)	
			144.72 (s, OC_6H_4O)	
			195.43 (d, J_{PC} = 23.1 Hz, CO)	
4b	2055	5.44 (d, J_{PH} = 1.7 Hz, 5H, C_5H_5)	87.94 (d, J_{PC} = 2.4 Hz, C_5H_5)	47.35 (s)
	2004	7.26 (s, 4H, $OC_{10}H_6O$)	105.53 (d, J_{PC} = 9.8 Hz, $OC_{10}H_6O$)	
		7.28−7.36 (m, 4H, $OC_{10}H_6O$)	124.04 (s, $OC_{10}H_6O$)	
		7.64−7.74 (m, 4H, $OC_{10}H_6O$)	126.97 (s, $OC_{10}H_6O$)	
			130.01 (s, $OC_{10}H_6O$)	
			144.60 (s, $OC_{10}H_6O$)	
			195.06 (d, J_{PC} = 24.4 Hz, CO)	
4c[c]	2051	2.28 (s, CH_3)	15.20 (s, CH_3)	46.40 (s)
	1999	2.29 (s, CH_3)	15.26 (s, CH_3)	47.11 (s)
		5.40 (d, J_{PH} = 1.7 Hz, C_5H_5)	87.89 (d, J_{PC} = 2.4 Hz, C_5H_5)	
		5.41 (d, J_{PH} = 1.7 Hz, C_5H_5)	107.76 (d, J_{PC} = 9.8 Hz, $OC_6H_3(CH_3)O$)	
		6.65−6.85 (m, $OC_6H_3(CH_3)O$)	108.02 (d, J_{PC} = 11.0 Hz, $OC_6H_3(CH_3)O$)	
			119.86 (s, $OC_6H_3(CH_3)O$)	
			120.13 (s, $OC_6H_3(CH_3)O$)	
			120.19 (d, J_{PC} = 8.5 Hz, $OC_6H_3(CH_3)O$)	
			120.40 (d, J_{PC} = 9.8 Hz, $OC_6H_3(CH_3)O$)	
			122.48 (s, $OC_6H_3(CH_3)O$)	
			122.88 (s, $OC_6H_3(CH_3)O$)	
			143.14 (s, $OC_6H_3(CH_3)O$)	
			143.45 (s, $OC_6H_3(CH_3)O$)	
			143.86 (d, J_{PC} = 2.4 Hz, $OC_6H_3(CH_3)O$)	
			144.29 (d, J_{PC} = 2.4 Hz, $OC_6H_3(CH_3)O$)	
			195.75 (d, J_{PC} = 23.2 Hz, CO)	
			195.78 (d, J_{PC} = 23.2 Hz, CO)	
			195.80 (d, J_{PC} = 23.1 Hz, CO)	

[a] In CD_2Cl_2. [b] In acetone-d_6. [c] **4c** is comprised of at least two isomers, and spectral assignment to a particular isomer is not attempted.

the corresponding metallaphosphorane. However, this method seems not to be appropriate for ruthenium phosphoranes, because of formation of some byproducts which makes the purification of ruthenium phosphoranes difficult. This made the yield of these ruthenium phosphoranes less than 20%.

Spectroscopic Data. Table 1 summarizes the IR (ν_{CO}), ^1H NMR, ^{13}C NMR, and ^{31}P NMR data for

Table 2. Comparison of Spectroscopic Data for Fe and Ru Complexes

complexes	M	IR: ν(CO) (cm^{-1})[a]		^{1}H NMR: Cp, δ (ppm)[b]	^{31}P NMR: δ (ppm)[b]
$[Cp(CO)_2M\{P(OC_6H_4NH)_2\}]$	Ru (**2a**)	2037	1983	5.38	0.66
	Fe[c]	2026	1977	4.94	25.67
$[Cp(CO)_2M\{P(OC_6H_4NMe)_2\}]$	Ru (**2b**)	2036	1983	5.38	−6.93
	Fe[c]	2024	1975	4.86	15.95
$[Cp(CO)_2M\{P(OC_6H_4O)_2\}]$	Ru (**4a**)	2052	2001	5.41	47.35
	Fe[c]	2042	1996	5.04	73.43

[a] In THF. [b] In $CDCl_3$. [c] Reference 10.

ruthenium complexes isolated in this study. A comparison of these data shows distinct differences between complexes **2** and **4**; the former contains two O substituents in apical positions and two N substitutents in equatorial positions on the P atom, while the latter contains only four O substitutents. In the IR spectra, two CO absorptions of **4** were observed at higher frequencies both by ca. 15 cm^{-1} than those of **2**. It is believed that the π back-donation from the filled M (d_π) orbital to the σ^* orbital of apical P−O bonds is one of the most important factors to stabilize the M−P bond in the metallaphosphorane complexes.[6] Therefore, the IR frequency differences are considered to come from the π acidity of the σ^* orbital, as follows. Since **4** has four electronegative O atoms on P, the electron density on P is reasonably expected to be lower in **4**. This is supported by the ^{31}P NMR spectra; the resonance is observed at a lower field for **4**. Thus, the stronger π back-donation (stronger π acidity of the σ^*) expected for **4** leads to lower electron density on Ru in **4**, thereby causing higher ν_{CO} frequencies for **4**.

The ^{13}C NMR data provide information on the behavior of phosphorane complexes in solution. For **2a**, two doublets due to carbonyl carbons at 197.98 and 198.20 ppm with a coupling constant of 22.1 and 22.0 Hz, respectively, were observed, which indicates the two carbonyls are diastereotopic. The similar results were obtained for **2b**. Since **2b** is demonstrated to have a trigonal-bipyramidal geometry around the phosphorus by its X-ray analysis (vide infra), **2a** is also expected to have a trigonal-bipyramidal geometry with two oxygen atoms in apical positions. It is highly likely that the racemization of those phosphoranes, if possible, takes place by Berry pseudorotation. If the pseudorotation on the pentacoordinate phosphorus should not occur, the phosphorane P would be a chiral center. Therefore, the above-mentioned results indicate that the pseudorotation does not take place either for **2a** or **2b** on the NMR time scale. Complexes **2a**,**b** require five transformation pathways to complete the racemization. During these pathways some tbp configurations have to have an equatophilic amino and/or ruthenium group in apical position(s), and in addition, they have to have a five-membered chelate ring connecting two equatorial positions. Therefore, when the rings contain N and O atoms bonded to phosphorus, like in **2a**,**b**, high-energy intermediates are encountered during racemization by an intramolecular process.

In contrast, only one signal assigned to carbonyl carbons was observed for **4a**,**b** in the ^{13}C NMR, and this result suggests that the pseudorotation does occur in **4** on the NMR time scale. This is because the racemization of **4** is attained by only one transformation pathway where the ruthenium fragment retains an equatorial position as a pivotal group. The lower energy barrier of the pseudorotation process for **4** is interpreted in this way. Detailed arguments about the pseudorotation process in **4** are described later.

To investigate the bond character between a transition metal and a hypervalent phosphorus atom in $[Cp(CO)_2Ru\{P(OC_6H_4E)_2\}]$ (E = O, NH, NMe), we compared their spectroscopic data with those of the Fe analogues[10] (see Table 2). The following observations suggest that the Ru−P bond is more polarized as $M^{\delta+}-P^{\delta-}$ than the Fe−P bond: (i) In the ^{31}P NMR spectra, the Ru complexes exhibit a signal at a ca. 24 ppm higher magnetic field than the iron complexes. It can be thus considered that the electron density on the phosphorus atom is higher in the Ru complexes. (ii) For the Ru complexes, the signal due to the Cp protons in the ^{1}H NMR spectrum appears at a ca. 0.4 ppm lower magnetic field, and the CO absorption bands in the IR spectrum appear at a ca. 10 cm^{-1} higher frequency, than those of the corresponding iron complexes. These results indicate that the electron density on the central metal is lower in Ru complexes. The same tendency has been reported for the related phosphonate complexes $[Cp(CO)_2M\{P(O)R^1R^2\}]$ (M = Ru, Fe; R^1 and/or R^2 = OMe, NC_4H_8),[17] which also have a metal−phosphorus(V) covalent bond. Therefore, the larger $M^{\delta+}-P^{\delta-}$ polarization for Ru than for Fe seems to be general.

Crystal Structures of 2b, 4b, and 3. X-ray structure analyses of **2b**, **4b**, and **3** were undertaken. The ORTEP drawings of them are displayed in Figures 1−3, and the crystal data and the selected bond distances and angles are listed in Tables 3−6.

The X-ray structures of **2b**, **4b**, and **3** show that the ruthenium takes a normal piano stool configuration with a cyclopentadienyl ligand in η^5 fashion, two terminal CO ligands, and a phosphorus ligand as a pentacoordinate phosphorus for **2b** and **4b** and as a normal phosphite for **3**. For both **2b** and **4b**, the five-coordinate phosphorus adopts a distorted trigonal-bipyramidal (tbp) geometry, but the degree of the distortion is different. With **2b**, the two apical bonds slightly bend away from the ruthenium fragment (the $O_{ap}-P-O_{ap}$ angle is 175.9°), and in the equatorial plane, the angles of $Ru-P-N_{eq}$ (121.7 and 123.7°) are slightly greater than the ideal angle (120°), though the sum of the equatorial angles is 359.9°. Those structural features are the same as those of the corresponding iron complex, $Cp(CO)_2Fe\{P(OC_6H_4NMe)_2\}$.[10b] In contrast, with **4b**, the two apical bonds largely bend from 180° (the $O_{ap}-P-O_{ap}$ angle is 158.0°), and in the equatorial

(17) (a) Nakazawa, H.; Fujita, T.; Kubo, K.; Miyoshi, K. *J. Organomet. Chem.* **1994**, *473*, 243. (b) Nakazawa, H., Kubo, K.; Tanisaki, K.; Kawamura, K.; Miyoshi, K. *Inorg. Chim. Acta* **1994**, *222*, 123.

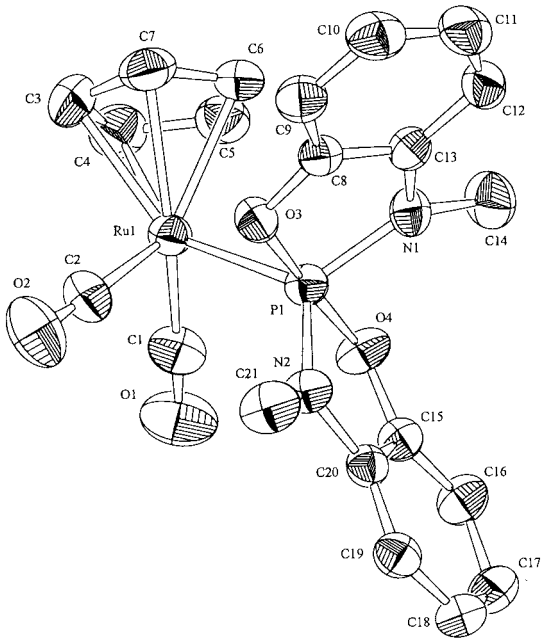

Figure 1. ORTEP drawing of **2b** (50% probability ellipsoids), showing the numbering system. All hydrogen atoms are omitted for clarity.

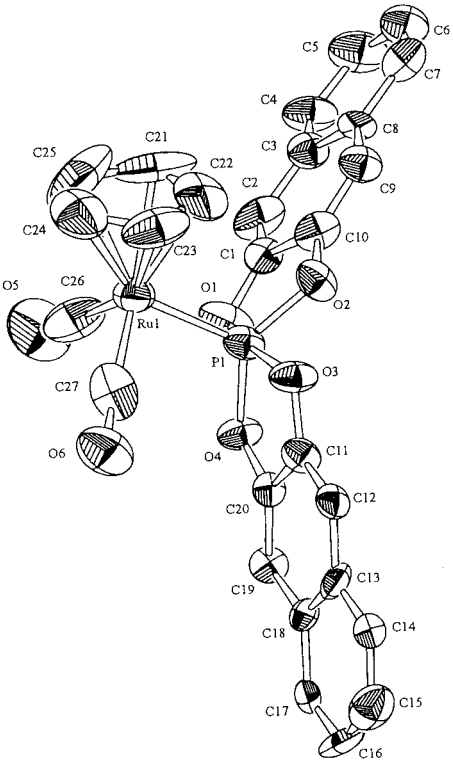

Figure 2. ORTEP drawing of **4b** (40% probability ellipsoids), showing the numbering system. All hydrogen atoms are omitted for clarity.

plane, the angles of Ru−P−O_{eq} (113.5 and 117.6°) are slightly smaller (not greater) than the ideal angle (120°), though the sum of the equatorial angles is 360.0°.

The structures for many spiro-phosphorane compounds of the type $RP(C_6H_4E_2)_2$ (R, E = main-group moiety) have been reported, and the degree of distortion from tbp to square pyramidal (sp) has been estimated by Holmes et al.[18] The difference between the ideal and observed structures is described as a percent value (an ideal tbp geometry corresponds to 0%, and an ideal sp geometry corresponds to 100%). Application of this method[9a] to our ruthenium phosphorane complexes provides 20.0% and 36.5% for **2b** and **4b**, respectively, indicating that **4b** is distorted from tbp approximately twice as much as **2b**. The difference may arise from a strong equatophilicity of an amino group (vide infra).

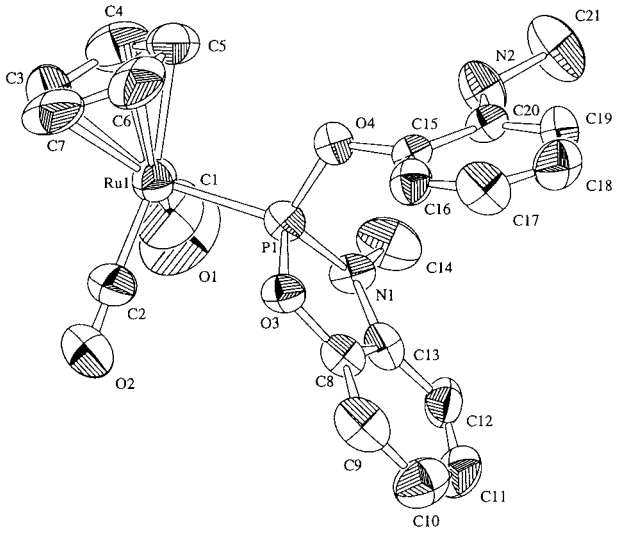

Figure 3. ORTEP drawing of **3** (50% probability ellipsoids), showing the numbering system. All hydrogen atoms and the BF_4^- counterion are omitted for clarity.

The geometries around nitrogens in **2b** are both planar (sums of the angles around N1 and N2 are 359.7 and 358.9°, respectively). The O3−P1−O4 bond is almost in both of the planes. Therefore, each nitrogen assumes sp^2 hybridization and the lone-pair electrons lie on the equatorial plane, implying favorable π donation of the lone-pair electrons to equatorial σ^* orbitals on the phosphorus. This interaction is proposed also for the corresponding iron phosphorus complexes[10] and is responsible for equatophilicity of an amino group and presumably for a smaller deviation from a tbp structure in terms of a phosphorane phosphorus.

The Ru−P bonds in **2b** and **4b** are 2.377(1) and 2.311(4) Å long, respectively. They are longer than the corresponding Fe−P bonds simply due to a large Ru van der Waals radius. The interesting point is that the Ru−P bond is clearly longer (by 0.066 Å) in **2b** than in **4b**. This is consistent with the suggestion reported previously that, in terms of an M(transition metal)−P(phosphorane) bond, π back-donation from M to P is a more important contributor than σ donation from P to M.[10b] This is supported by the fact that the 0.066 Å difference in M−P bond distance between **2b** and **4b** is larger than the corresponding 0.020 Å difference between an iron phosphorane complex containing two amino and two alkoxy groups and an iron complex containing one amino and three alkoxy groups. That is, the difference in π acidity of the P fragment is larger between **2b** and **4b** than between the two iron complexes. Another support comes from the IR data. The ν_{CO} stretching bands of **4b** (2055 and 2004 cm^{-1}) are at a ca. 20 cm^{-1} higher frequency than those of **2b** (2036 and 1983 cm^{-1}), while those of the former iron complex

(18) (a) Holmes, R. R. *Acc. Chem. Res.* **1979**, *12*, 257. (b) Holmes, R. R.; Deiters, J. A. *J. Am. Chem. Soc.* **1977**, *99*, 3318.

Table 3. Summary of Crystal Data for 2b, 4b, and 3

	2b	4b	3
formula	$C_{21}H_{19}N_2O_4PRu$	$C_{27}H_{17}O_6PRu$	$C_{21}H_{20}BF_4N_2O_4PRu$
fw	495.44	569.47	583.25
cryst syst	monoclinic	orthorhombic	monoclinic
spece group	*P*2/c	$P2_12_12_1$	$P2_1/n$
cell constants			
a, Å	13.185(2)	16.033(5)	12.716(2)
b, Å	7.278(2)	7.019(2)	15.028(4)
c, Å	20.987(2)	20.277(5)	13.221(3)
α, deg			
β, deg	90.38(1)		107.49(2)
γ, deg			
V, Å^3	2014(1)	2282(1)	2410(1)
Z	4	4	4
D_{calcd}, g cm^{-3}	1.63	1.66	1.61
μ, cm^{-1}	8.89	8.01	7.78
cryst size, mm	0.75 × 0.63 × 0.45	0.60 × 0.13 × 0.07	0.12 × 0.10 × 0.10
radiation (*λ*, Å)	Mo Kα (0.710 73)	Mo Kα (0.710 73)	Mo Kα (0.710 73)
scan technique	*ω*	*ω*	*ω*
scan range, deg	$3 < 2\theta < 55$	$3 < 2\theta < 53$	$3 < 2\theta < 55$
scan rate, deg min^{-1}	6.0	6.0	6.0
no. of unique data	5048	4476	5753
no. of unique data with $F_o > 3\sigma(F_o)$	3963	1877	1656
R	0.027	0.048	0.058
R_w	0.036	0.035	0.047

Table 4. Selected Bond Distances (Å) and Angles (deg) for 2b

	Bond Distances		
Ru1−P1	2.377(1)	O3−C8	1.357(2)
Ru1−C1	1.869(3)	O4−C15	1.365(3)
Ru1−C2	1.878(3)	N1−C13	1.399(3)
P1−O3	1.771(2)	N1−C14	1.450(3)
P1−O4	1.752(2)	N2−C20	1.397(3)
P1−N1	1.721(2)	N2−C21	1.459(3)
P1−N2	1.716(2)	C8−C13	1.390(3)
O1−C1	1.142(3)	C15−C20	1.389(3)
O2−C2	1.134(4)		
	Bond Angles		
P1−Ru1−C1	91.47(8)	P1−O3−C8	114.2(1)
P1−Ru1−C2	87.04(8)	P1−O4−C15	113.2(1)
C1−Ru1−C2	91.8(1)	P1−N1−C13	114.7(1)
Ru1−P1−O3	89.57(5)	P1−N1−C14	127.4(2)
Ru1−P1−O4	94.50(6)	C13−N1−C14	117.6(2)
Ru1−P1−N1	121.65(7)	P1−N2−C20	114.1(2)
Ru1−P1−N2	123.65(7)	P1−N2−C21	128.0(2)
O3−P1−O4	175.92(8)	C20−N2−C21	116.8(2)
O3−P1−N1	87.25(8)	O3−C8−C13	112.2(2)
O3−P1−N2	90.46(9)	N1−C13−C8	111.2(2)
O4−P1−N1	90.38(9)	O4−C15−C20	112.3(2)
O4−P1−N2	87.51(8)	N2−C20−C15	110.6(2)
N1−P1−N2	114.63(9)		

Table 5. Selected Bond Distances (Å) and Angles (deg) for 4b

	Bond Distances		
Ru1−P1	2.311(4)	O2−C10	1.38(1)
Ru1−C26	1.89(2)	O3−C11	1.35(1)
Ru1−C27	1.87(2)	O4−C20	1.39(1)
P1−O1	1.758(9)	O5−C26	1.12(2)
P1−O2	1.659(8)	O6−C27	1.15(2)
P1−O3	1.734(7)	C1−C10	1.42(2)
P1−O4	1.673(9)	C11−C20	1.39(1)
O1−C1	1.36(1)		
	Bond Angles		
P1−Ru1−C26	90.1(5)	O2−P1−O4	128.9(4)
P1−Ru1−C27	90.3(5)	O3−P1−O4	89.3(4)
C26−Ru1−C27	91.5(6)	P1−O1−C1	114.5(8)
Ru1−P1−O1	101.8(3)	P1−O2−C10	115.2(9)
Ru1−P1−O2	113.5(3)	P1−O3−C11	113.6(7)
Ru1−P1−O3	100.2(3)	P1−O4−C20	113.8(7)
Ru1−P1−O4	117.6(3)	O1−C1−C10	109(1)
O1−P1−O2	87.6(4)	O2−C10−C1	112(1)
O1−P1−O3	158.0(4)	O3−C11−C20	111(1)
O1−P1−O4	81.6(4)	O4−C20−C11	112(1)
O2−P1−O3	82.5(4)		

are at a ca. 10 cm^{-1} higher frequency than those of the latter iron complex.[10b]

Another interesting structural feature is the orientation of the phosphorane ligand in crystals of **2b** and **4b**. The Ru1−P1−O3−O4 least-squares mean plane in **2b** is situated between Cp and two COs, and torsion angles are 30.3° for C1−Ru1−P1−O3 and 57.7° for C2−Ru1−P1−O4 (Figure 4a). Similar values are observed for **4b**, 33.3° for C26−Ru1−P1−O1 and 56.7° for C27−Ru1−P1−O3 (Figure 4b). The σ^* orbital of the apical 3-center 4-electron bond on the P is situated such that it nicely overlaps with the HOMO of the $Cp(CO)_2Ru$ fragment which is expected to be similar in shape to that of the $Cp(CO)_2Fe$ fragment reported by Hoffmann et al. (Figure 4c).[19] As a result, the orientations of the phosphorane ligand revealed by the X-ray analyses are favorable for the σ^* orbital of the 3c−4e bond to accept electron density from the HOMO of the $Cp(CO)_2Ru$ fragment.

The X-ray structure of **3** (Figure 3) reveals that **3** is a normal ruthenium complex containing an amino-substituted phosphite. In this complex, no transannular interaction is observed between N2 and P1.

Berry Pseudorotation Process of Ruthenium Phosphorane. To investigate a pseudorotation process of a transition-metalated phosphorane in more detail, we prepared **4c**, which has two 3-methylcatecholate substituents in addition to a $Cp(CO)_2Ru$ fragment on a phosphorane phosphorus. Scheme 5 shows a graph for possible isomers of **4c** and the relationship among them through Berry pseudorotation according to the convention.[20] A brief explanation about Scheme 5 may be pertinent. The phosphorus in **4c** is surrounded by Ru and two kinds of oxygens (O1 and O2, which are close

(19) (a) Schilling, B. E. R.; Hoffmann, R.; Lichtenberger, D. L. *J. Am. Chem. Soc.* **1979**, *101*, 585. (b) Schilling, B. E. R.; Hoffmann, R.; Faller, J. W. *J. Am. Chem. Soc.* **1979**, *101*, 592.

(20) Emsley, J.; Hall, D. In *The chemistry of Phosphorus*; Harper & Row: New York, 1976.

Table 6. Selected Bond Distances (Å) and Angles (deg) for 3

	Bond Distances		
Ru1−P1	2.265(4)	O3−C8	1.39(2)
Ru1−C1	1.89(2)	O4−C15	1.42(1)
Ru1−C2	1.84(2)	N1−C13	1.39(2)
P1−O3	1.618(8)	N1−C14	1.47(2)
P1−O4	1.594(8)	N2−C20	1.40(2)
P1−N1	1.66(1)	N2−C21	1.45(2)
O1−C1	1.14(2)	C8−C13	1.39(2)
O2−C2	1.18(2)	C15−C20	1.39(2)
	Bond Angles		
P1−Ru1−C1	94.8(6)	P1−O4−C15	122.3(8)
P1−Ru1−C2	89.0(5)	P1−N1−C13	113.8(8)
C1−Ru1−C2	90.3(8)	P1−N1−C14	126(1)
Ru1−P1−O3	114.4(3)	C13−N1−C14	120(1)
Ru1−P1−O4	109.7(4)	C20−N2−C21	120(1)
Ru1−P1−N1	124.1(3)	O3−C8−C13	114(1)
O3−P1−O4	105.4(4)	N1−C13−C8	107(1)
O3−P1−N1	92.8(5)	O4−C15−C20	120(1)
O4−P1−N1	108.2(4)	N2−C20−C15	118(1)
P1−O3−C8	111.4(7)		

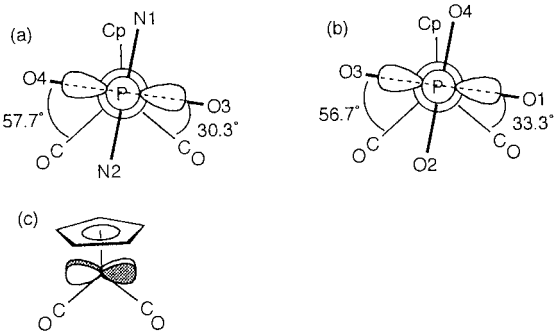

Figure 4. (a) Newman projection along the P1−Ru1 bond for **2b**. (b) Newman projection along the P−Ru bond for **4b**. (c) HOMO of the $Cp(CO)_2Fe$ fragment.

to and far from the methyl substituent, respectively). A symbol in an oval is to denote a particular tbp configuration by the apical atoms. An italicized symbol shows the optical isomer of the parent compound. An atom drawn between symbols next to each other shows a pivot ligand about which pseudorotation converts one isomer into another. For complex **4c**, there are 10 possible configurations which can be linked by 11 Berry pseudorotations.

A white powder isolated from the reaction of **1** with 3-methylcatechol in the presence of Et_3N is a mixture of some isomers of **4c**. The ^{31}P NMR spectrum at room temperature shows two singlets with an integration ratio of 1:1.17 at 47.11 and 46.40 ppm, respectively, which are in the range of ruthenium−phosphorane complexes. Because of equatophilicity of a transition-metal fragment and no report of a metalated phosphorane with a transition-metal fragment in an apical position, only six isomers, all of which have the ruthenium fragment in an equatorial position, can be considered as possible isomers of the isolated **4c**. **4c**-O1O1 vs **4c**-*O2O2*, **4c**-O1O2 vs **4c**-*O1O2*, and **4c**-O2O2 vs **4c**-*O1O1* are interconvertible by one transformation pathway with the Ru fragment in an equatorial position as a pivotal group. Therefore, two isomers in each pair are not distinguished in NMR spectra at room temperature. The interconversion between **4c**-O1O2 and **4c**-*O1O2* corresponds to enantiomerization. **4c**-O1O1/*O2O2* is enantiomeric to **4c**-*O1O1*/O2O2, but they are not interconvertible to each other because the inversion requires

Scheme 5

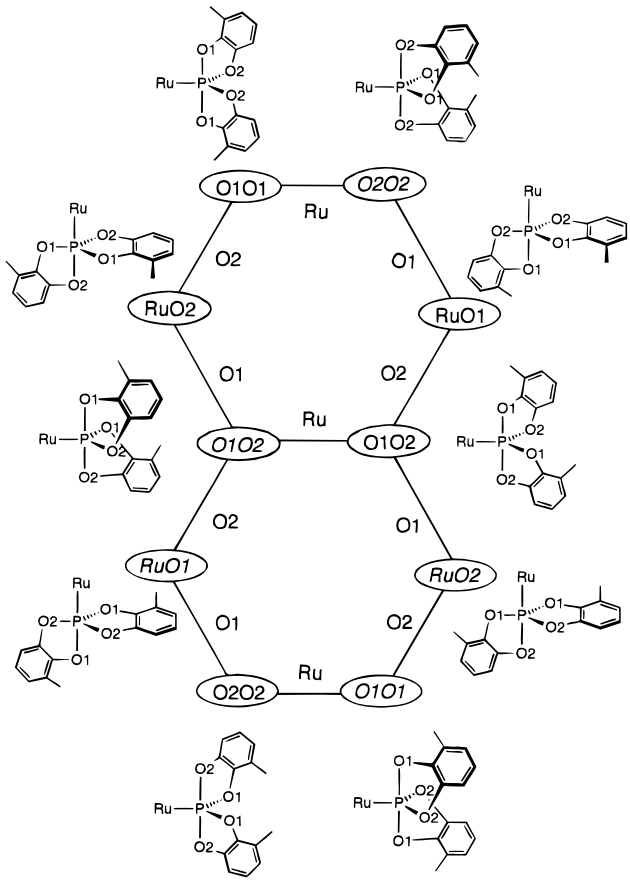

4 transformation pathways via two structures which have a Ru fragment in an apical position. Therefore, the two signals observed in the ^{31}P NMR may be attributed to **4c**-O1O1/*O2O2*/*O1O1*/O2O2 and **4c**-O1O2/*O1O2*.

The rotational feature mentioned above is further supported by the ^{13}C NMR data. The isolated **4c** shows three doublets due to CO carbons at 195.80, 195.78, and 195.75 ppm. Since the **4c**-O1O2/*O1O2* conversion accompanies disappearance of chirality at the phosphorus, **4c**-O1O2/*O1O2* gives one doublet assigned to CO. In contrast, during the **4c**-O1O1/*O2O2* conversion and equally the **4c**-*O1O1*/O2O2 conversion, the phosphorus chirality is not lost. Therefore, two carbonyl groups in the $Cp(CO)_2Ru$ fragment are diastereotopic, giving rise to two doublets in the ^{13}C NMR spectra.

The variable-temperature ^{31}P NMR data provide further information on the isomerization. As mentioned above, **4c**-O1O1/*O2O2* and **4c**-*O1O1*/O2O2 show the identical ^{31}P NMR chemical shift, and **4c**-O1O2/*O1O2* shows another singlet at room temperature. Even at 183 K the ^{31}P NMR spectrum shows two singlets, indicating that energy barriers of pseudorotation between **4c**-O1O1 and **4c**-*O2O2* (equally between **4c**-*O1O1* and **4c**-O2O2), and between **4c**-*O1O2* and **4c**-O1O2 are very small. In contrast, the two singlets coalesce into one broad resonance at 340 K and then sharpened to one singlet at higher temperatures (Figure 5). This means that isomerization between **4c**-O1O1/*O2O2* and **4c**-O1O2/*O1O2* (equally between **4c**-*O1O1*/O2O2 and **4c**-O1O2/*O1O2*) takes place faster than the NMR time scale at temperatures higher than 340 K.

The first-order rate constant for the isomerization between **4c**-O1O1/*O2O2* and **4c**-O1O2/*O1O2* (equally

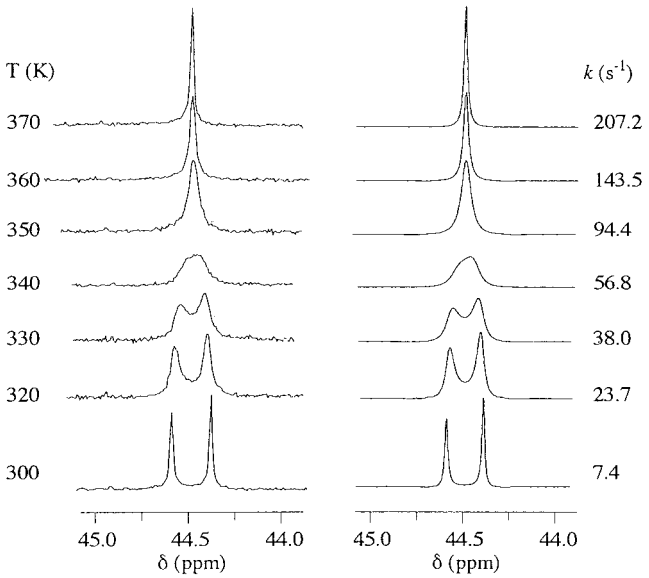

Figure 5. 121.50 MHz variable-temperature experimental (left) and simulated (right) ^{31}P NMR spectra of **4c**.

between **4c**-*O1O1*/O2O2 and **4c**-O1O2/*O1O2*) can be estimated by a line-shape analysis.[21] Simulation of VT-NMR spectrum is displayed in Figure 5. From application of coalescence formulas,[22] the activation parameters were obtained: $\Delta H^{\ddagger} = 42.1 \pm 0.5$ kJ mol^{-1}; $\Delta S^{\ddagger} = -91.1 \pm 1.6$ J mol^{-1} K^{-1}; $\Delta G_{340}^{\ddagger} = 73.1 \pm 0.7$ kJ mol^{-1}. These small $\Delta H^{\ddagger}$ and $\Delta S^{\ddagger}$ values suggest that the isomerization proceeds through the pseudorotation process but not the mechanism involving cleavage of a P−O bond. The activation parameters obtained here correspond to the isomerization between **4c**-O1O1/*O2O2* and **4c**-O1O2/*O1O2* (equally between **4c**-*O1O1*/O2O2 and **4c**-O1O2/*O1O2*), which consists of two Berry pseudorotation pathways. One involves the Ru fragment movement from an equatorial to an apical position, and the other involves the movement from an apical to an equatorial position. Therefore, it can be said that the activation parameters obtained here correspond to the former pathway. This is, to our knowledge, the first report of activation parameters of Berry pseudorotation for a metallaphosphorane.

Acknowledgment. This work was supported by a Grant-in-Aid for Science Research (Grant No. 10440195) and a Grant-in Aid on Priority Area of Interelement Chemistry (No. 09239235) from the Ministry of Education, Science, Sports, and Culture of Japan.

Supporting Information Available: Tables giving positional and thermal parameters and bond distances and angles for **2b**, **4b**, and **3** (20 pages). This material is available free of charge via the Internet at http://pubs.acs.org.

OM990044K

(21) (a) DNMR5: Stephenson, D. S.; Binch, G. Program 365, Quantum Chemistry Program Exchange, Indiana University, Bloomington, IN 47405. (b) DNMR5 (IBM-PC version): LeMaster, C. B.; LeMaster, C. L.; True, N. S. Program QCMP 059, Quantum Chemistry Program Exchange, Indiana University, Bloomington, IN 47405.

(22) Sandström, J. In *Dynamic NMR Spectroscopy*; Academic Press: New York, 1982; Chapters 2 and 7.